

Gravastar Shadows

Nobuyuki Sakai*

Faculty of Science, Yamaguchi University, Yamaguchi 753-8512, Japan

Hiromi Saida†

Department of Physics, Daido University, Minami-ku, Nagoya 457-8530, Japan

Takashi Tamaki‡

*Department of Physics, General Education, College of Engineering,
Nihon University, Tokusada, Tamura, Koriyama, Fukushima 963-8642, Japan*

Direct observation of black holes is one of the grand challenges in astronomy. If there are super-compact objects which possess unstable circular orbits of photons, however, it may be difficult to distinguish them from black holes by observing photons. As a model of super-compact objects, we consider a gravastar (gravitational-vacuum-star) which was originally proposed by Mazur and Mottola. For definiteness, we adopt a spherical thin-shell model of a gravastar developed by Visser and Wiltshire, which connects interior de-Sitter geometry and exterior Schwarzschild geometry. We find that unstable circular orbits of photons can appear around the gravastar. Then, we investigate the optical images of the gravastar possessing unstable circular orbits, with assuming the optically transparent surface of it and two types of optical sources behind the gravastar: (i) an infinite optical plane and (ii) a companion star. The main feature of the image of (i) is that a bright disk and a dark thick ring surrounding the disk appear in the center of the region which would be completely dark if the compact object was not the gravastar but Schwarzschild black hole. Also in the case (ii), a small disk and arcs around the disk appear in the region which would be completely dark for the lensing image by Schwarzschild black hole. Because characteristic images appear inside the gravastar in both cases, we could tell the difference between a black hole and a gravastar with high-resolution VLBI observations near future.

PACS numbers: 04.40.Dg, 97.60.Lf, 97.60.Lf

I. INTRODUCTION

Direct observation of black holes is one of the grand challenges in astronomy and will be achieved by VLBI observations in the near future [1]. In such an observation, we expect to observe the images of optical/radio sources around a black hole, which is called black-hole shadows. In black-hole spacetimes such as Schwarzschild spacetime, there exist unstable circular orbits of photons, which play an important role generating shadows. First, if optical sources are extended behind a black hole, one cannot detect photons which have passed inside the unstable circular orbits because any photon passing the unstable circular orbits inward eventually falls into the event horizon. Second, because null geodesics wind several times in the vicinity of unstable circular orbits, one could observe brightening there when gas falls into the black hole. Therefore, the direct observation of black holes usually means observation of geometry in the vicinity of unstable circular orbits of photons.

These natures naturally give rise to a question: are there any super-compact objects which possess unstable circular orbits of photons? If such super-compact objects exist, one cannot claim to have seen a black hole even if one observes temporal brightening of gas falling into the

object. Therefore, it is important to study the possibility of super-compact objects and their observational consequences.

As a model of super-compact objects, we consider a model of gravastars. Gravastars were originally proposed by Mazur and Mottola [2] as a new final state of gravitational collapse of stars, that is, an alternative to black holes. In this model an interior de Sitter region and an exterior Schwarzschild background are connected by a shell of stiff matter ($p = \rho$). Although their formation process is unclear, the idea is fascinating because it could solve two fundamental problems of black holes: singularity problem and information loss paradox.

As we shall show in Sec. II, we find that some gravastar solutions possess unstable circular orbits of photons. This result indicates that it is difficult to distinguish those gravastars from black holes. Chirenti and Rezzolla [3] considered a question of how to tell a gravastar from a black hole. They studied axial-perturbations on gravastars and found that their quasi-normal modes of gravitational waves differ from those of black holes. Broderick and Narayan [4] argued that, if observed black hole candidates with matter accretion were gravastars, they should heat up and emit radiation. With this thermal process they discussed observational constraints on gravastar models.

In this paper we tackle the same question in a different approach: can we tell a gravastar from a black hole by electromagnetic observations instead of gravitational wave observations? Obviously the answer depends on the state of the surface: there are three possibilities.

*Electronic address: nsakai@yamaguchi-u.ac.jp

†Electronic address: saida@daido-it.ac.jp

‡Electronic address: tamaki@ge.ce.nihon-u.ac.jp

- The surface emits electromagnetic waves. In this case one could detect the electromagnetic waves, and hence a gravastar can be distinguished from a black hole observationally.
- The surface is black and does not emit electromagnetic waves. In this case there is no chance to identify a gravastar.
- The surface is electromagnetically transparent.

Observational consequences in the last case is not clear and potentially important. Therefore, we investigate observational images of the gravastar under the assumption that the surface is electromagnetically transparent.

This paper is organized as follows. In Sec. II, we re-analyze the thin-shell model of a gravastar and search stable solutions systematically. In Sec. III, we derive null geodesic equations and find solutions which possess unstable circular orbits of photons. In Sec. IV, we solve the null geodesic equations numerically to obtain the images of optical sources behind the gravastar. Section V is devoted to concluding remarks.

II. THIN-SHELL MODEL

We consider the spherical thin-shell model of a gravastar developed by Visser and Wiltshire [5]. Here we adopt their model. The inside is a part of de Sitter spacetime,

$$ds^2 = -A_- dt_-^2 + \frac{dr_-^2}{A_-} + r_-^2 (d\theta^2 + \sin^2 \theta d\varphi^2),$$

with $A_-(r_-) \equiv 1 - H^2 r_-^2$,

(2.1)

and the outside is a part of Schwarzschild spacetime,

$$ds^2 = -A_+ dt_+^2 + \frac{dr_+^2}{A_+} + r_+^2 (d\theta^2 + \sin^2 \theta d\varphi^2),$$

with $A_+(r_+) \equiv 1 - \frac{r_g}{r_+}$,

(2.2)

where r_g is a gravitational radius. We have denoted field variables on the outside (inside) by superscripts or subscripts $+$ ($-$). To describe the geometry in the vicinity of the boundary hypersurface Σ , we introduce a Gaussian normal coordinate system,

$$\begin{aligned} ds^2 &= dn^2 + \gamma_{ij}^\pm x^i dx^j \\ &= dn^2 - \alpha_\pm(n, \tau)^2 d\tau^2 \\ &\quad + r_\pm(n, \tau)^2 (d\theta^2 + \sin^2 \theta d\varphi^2), \end{aligned}$$
(2.3)

in which $n = 0$ corresponds to Σ . α is normalized by $\alpha_\pm(0, \tau) = 1$ so that τ implies the proper time of Σ . $R(\tau) \equiv r_\pm(0, \tau)$ denotes the areal radius of Σ . We suppose that Σ contains infinitesimally thin matter,

$$S_j^i \equiv \int_{-0}^{+0} T_j^i dn = \text{diag}(-\sigma, \varpi, \varpi),$$
(2.4)

where σ and ϖ are the surface energy density and the surface pressure, respectively. Following Visser and Wiltshire [5], we assume 2+1 dimensional stiff matter:

$$\varpi = \sigma. \quad (2.5)$$

What we are looking for is static and stable solutions of a gravastar. As for their stability, we only consider stability against spherical perturbations. Stability against non-spherical perturbations is important as well, but it is beyond the present work. In the following we derive the equations of motion of the shell to find static and stable solutions.

Following the Israel's formalism [6, 7], we can obtain the junction conditions at Σ as follows. The metric continuity $\gamma_{ij}^+ = \gamma_{ij}^-$ implies

$$R = r_+ = r_-, \quad (2.6)$$

$$d\tau^2 = A_+ dt_+^2 - \frac{dr_+^2}{A_+} = A_- dt_-^2 - \frac{dr_-^2}{A_-}. \quad (2.7)$$

The other junction conditions are reduced to the two equations. One is

$$\beta_- - \beta_+ = 4\pi G\sigma R, \quad (2.8)$$

where

$$\beta_\pm \equiv \frac{\partial r_\pm}{\partial n} = \varepsilon_\pm \sqrt{\left(\frac{dR}{d\tau}\right)^2 + A_\pm}, \quad \varepsilon_\pm \equiv \text{sign} \frac{\partial r_\pm}{\partial n}. \quad (2.9)$$

In a spacetime without Schwarzschild horizon nor de Sitter horizon, $\varepsilon_\pm = +1$ because the areal radius r_\pm always increases as n increases. The other equation is

$$\frac{d}{d\tau}(\sigma R^2) + \varpi \frac{d}{d\tau}(R^2) = 0. \quad (2.10)$$

For stiff matter (2.5), we find

$$\sigma R^4 = \text{const.} \quad (2.11)$$

Introducing dimensionless quantities,

$$\begin{aligned} \tilde{R} &\equiv \frac{R}{r_g}, \quad \tilde{\tau} \equiv \frac{\tau}{r_g}, \\ h &\equiv r_g H, \quad s \equiv \frac{4\pi G\sigma R^4}{r_g^3} = \text{const.}, \end{aligned} \quad (2.12)$$

we rewrite (2.8) as

$$\left(\frac{d\tilde{R}}{d\tilde{\tau}}\right)^2 + U(\tilde{R}) = 0, \quad (2.13)$$

$$U(\tilde{R}) \equiv 1 - \frac{h^2 \tilde{R}^2}{2} - \frac{1}{2\tilde{R}} - \frac{s^2}{4\tilde{R}^6} - \frac{\tilde{R}^6}{4s^2} \left(h^2 \tilde{R}^2 - \frac{1}{\tilde{R}}\right)^2. \quad (2.14)$$

Figure 1 shows an example of the potential function $U(\tilde{R})$ which allows a static and stable solution. The red dot on the bold line represents a static solution. If

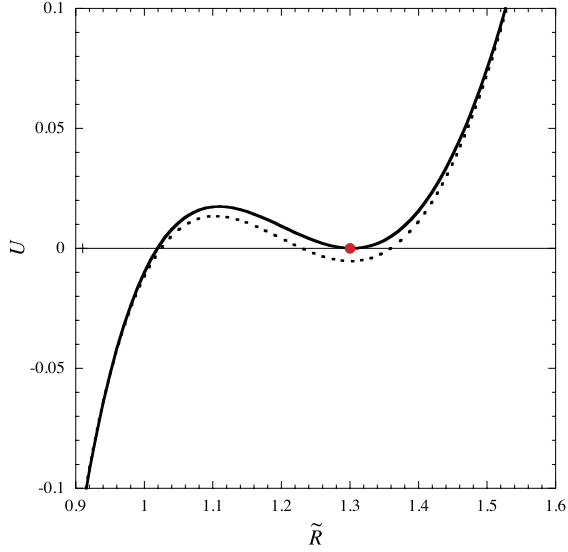


FIG. 1: Graph of the potential function $U(\tilde{R})$. The red dot on the bold line represents a static solution, where we put $h = 0.4$ and $s = 0.8212081$. If we give perturbations on the static solution by changing $r_g \rightarrow 1.003r_g$, we obtain the potential indicated by the dotted line. The perturbed potential allows an oscillating solution, which implies that the original static solution is stable.

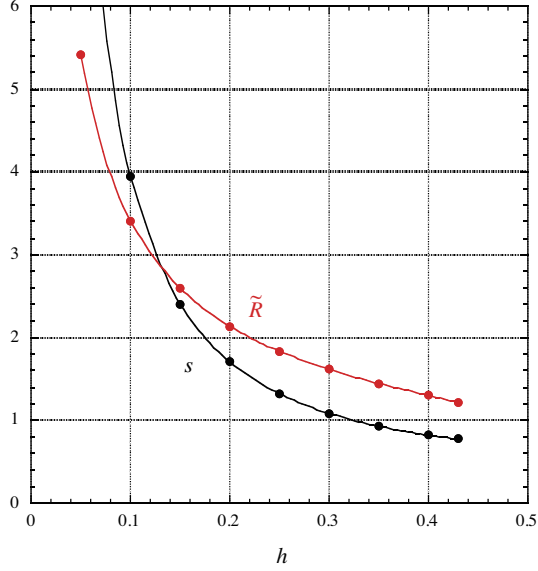


FIG. 2: Parameters s and \tilde{R} as a function of h , when $U(\tilde{R})$ has a local minimum on $U(\tilde{R}) = 0$ as shown in Fig. 1. Only these parameter values allow for static and stable gravastar solutions. h has an upper limit, $h_{\max} \approx 0.43$.

we give perturbations on the static solution by changing $r_g \rightarrow 1.003r_g$, we obtain the potential indicated by the dotted line. The perturbed potential allows an oscillating solution, which implies that the original static solution is stable against perturbations with increasing mass.

As Fig. 1 indicates, static and stable solutions exist if and only if $U(\tilde{R})$ has a local minimum on $U(\tilde{R}) = 0$. This condition gives a constraint on the three parameters

h , s and \tilde{R} . We survey static and stable solutions and show their parameters s and \tilde{R} as a function of h in Fig. 2. h has an upper limit, $h_{\max} \approx 0.43$, because the local minimum of $U(\tilde{R})$ disappears or cannot be located on $U(\tilde{R}) = 0$ when $h > h_{\max}$.

III. NULL GEODESIC EQUATIONS

In this section we derive null geodesic equations with boundary conditions for the static gravastar spacetime obtained in §II. We denote the affine parameter and the null vector by λ and $k^\mu = dx^\mu/d\lambda$, respectively; then the geodesic equations are generally expressed as

$$\frac{dk^\mu}{d\lambda} + \Gamma^\mu_{\nu\rho} k^\nu k^\rho = 0, \quad \text{with} \quad k_\mu k^\mu = 0. \quad (3.1)$$

The geodesics in the $\theta = \pi/2$ plane for the outside (+) and the inside (−) are given by

$$\frac{d}{d\lambda_\pm} (A_\pm k_\pm^t) = 0, \quad \frac{d}{d\lambda_\pm} (r_\pm^2 k_\pm^\varphi) = 0, \quad (3.2)$$

$$\frac{1}{\sqrt{A_\pm}} \frac{d}{d\lambda_\pm} \left(\frac{k_\pm^r}{\sqrt{A_\pm}} \right) + \frac{dA_\pm}{dr_\pm} \frac{(k_\pm^t)^2}{2} - r_\pm (k_\pm^\varphi)^2 = 0, \quad (3.3)$$

$$-A_\pm (k_\pm^t)^2 + \frac{(k_\pm^r)^2}{A_\pm} + r_\pm^2 (k_\pm^\varphi)^2 = 0. \quad (3.4)$$

Because Eq.(3.3) is also derived by (3.2) and (3.4), we do not have to solve it. Equations (3.2) are integrated as

$$A_\pm k_\pm^t = \text{const.} \equiv E_\pm, \quad r_\pm^2 k_\pm^\varphi = \text{const.} \equiv L_\pm, \quad (3.5)$$

and then (3.4) becomes

$$(k_\pm^r)^2 + \frac{A_\pm L_\pm^2}{r_\pm^2} = E_\pm^2. \quad (3.6)$$

It follows from (3.5) and (3.6) that

$$\frac{dr_\pm}{d\varphi} = \frac{k_\pm^r}{k_\pm^\varphi} = \frac{r_\pm^2 k_\pm^r}{L_\pm} = \pm r_\pm \sqrt{\left(\frac{E_\pm r_\pm}{L_\pm} \right)^2 - A_\pm}, \quad (3.7)$$

which gives null geodesics in the exterior and interior regions of the gravastar.

The equation for the interior region in (3.7) is integrated as

$$r_- = r_m \sec(\varphi - \varphi_m), \quad r_m \equiv \left(\frac{E_-^2}{L_-^2} + H^2 \right)^{-\frac{1}{2}}, \quad (3.8)$$

where φ_m is an integral constant. Since a black hole horizon does not exist and the surface of the gravastar is transparent in our situation, any incident light ray to the gravastar has to penetrate the gravastar, as shown in Fig. 3. Therefore, there are two crossing points of the penetrating null geodesic with the surface of gravastar Σ .

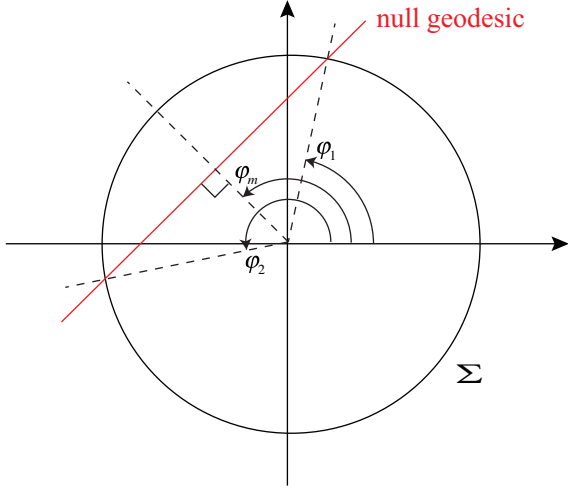


FIG. 3: Null geodesics penetrating the gravitar. φ_1 and φ_2 ($\varphi_1 < \varphi_2$) denote the two crossing points. The integral constant φ_m corresponds to the closest point to the center.

Let φ_1 and φ_2 ($\varphi_1 < \varphi_2$) denote the φ -coordinate values of those two crossing points, they are determined by

$$\varphi_m = \varphi_1 + \arccos \frac{r_m}{R} = \varphi_2 - \arccos \frac{r_m}{R}. \quad (3.9)$$

On the other hand, the equation for the exterior region in (3.7) cannot be integrated analytically. However, the asymptotic solution at $r \rightarrow \infty$ is obtained by putting $A_+ \rightarrow 1$:

$$r_+ = \frac{L_+}{E_+} \sec(\varphi - \varphi_c), \quad (3.10)$$

where φ_c is an integral constant.

Next, we discuss the boundary conditions of k^μ at Σ . In the case of a static gravitar, $R = \text{const.}$, the relation between the Gaussian normal coordinates (2.3) and the outer/inner coordinates (2.1) and (2.2) are given by

$$\begin{aligned} d\tau^2 &= A_+ dt_+^2 = A_- dt_-^2, \\ R^2 d\varphi^2 &= r_+^2 d\varphi^2 = r_-^2 d\varphi^2. \end{aligned} \quad (3.11)$$

Then we find

$$\sqrt{A_+} k_+^t = \sqrt{A_-} k_-^t, \quad k_+^\varphi = k_-^\varphi. \quad (3.12)$$

With the help of the null condition (3.4), we also obtain

$$\frac{k_+^r}{\sqrt{A_+}} = \frac{k_-^r}{\sqrt{A_-}}. \quad (3.13)$$

The relations among the integration constants are given by (2.6), (3.5) and (3.12),

$$L_+ = L_-, \quad \frac{E_+}{\sqrt{A_+}} = \frac{E_-}{\sqrt{A_-}}. \quad (3.14)$$

Hereafter we denote L_+ and L_- simply by L because they are identical.

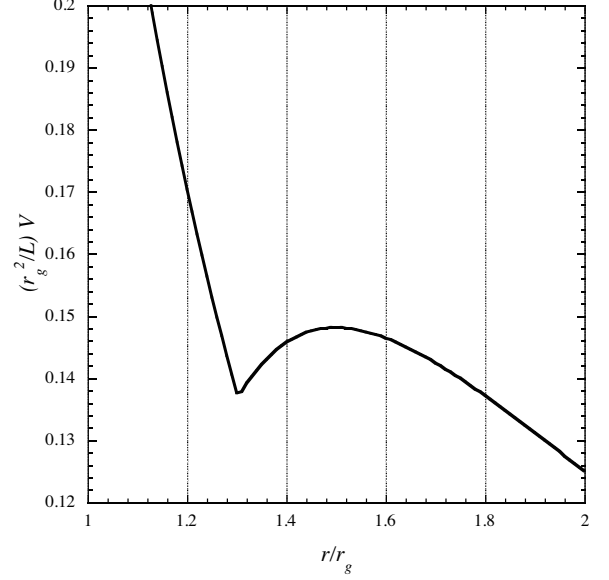


FIG. 4: Graph of the effective potential of null geodesics, $V(r)$, for the static solution with $h = 0.4$ ($\tilde{R} = 1.303$). There are a stable circular orbit at $r = R$ and an unstable circular orbit at $r = 1.5r_g$.

To make a qualitative discussion on photon trajectories, it is convenient to introduce the effective potential as follows. Equation (3.6) is rewritten as

$$\left(\frac{dr_\pm}{d\lambda_\pm} \right)^2 + \frac{L^2 A_\pm}{r_\pm^2} = E_\pm^2. \quad (3.15)$$

To discuss the dynamics with a continuous “potential” by analogy with the Newtonian mechanics, we introduce unified variables as

$$\begin{aligned} r = r_- \quad \text{and} \quad \lambda &= \sqrt{\frac{A_-(R)}{A_+(R)}} \lambda_- \quad (\text{inside}), \\ r = r_+ \quad \text{and} \quad \lambda &= \lambda_+ \quad (\text{outside}), \end{aligned} \quad (3.16)$$

and define the effective potential as

$$\begin{aligned} V(r < R) &= \frac{L^2 A_-}{r^2} \frac{A_+(R)}{A_-(R)} = L^2 \frac{A_+(R)}{A_-(R)} \left(\frac{1}{r^2} - H^2 \right), \\ V(r > R) &= \frac{L^2 A_+}{r^2} = L^2 \left(\frac{1}{r^2} - \frac{r_g}{r^3} \right). \end{aligned} \quad (3.17)$$

Then we obtain the continuous equation of motion,

$$\left(\frac{dr}{d\lambda} \right)^2 + V(r) = E_+^2. \quad (3.18)$$

Figure 4 shows the effective potential for the static solution with $h = 0.4$. There are a stable circular orbit at $r = R$ and an unstable circular orbit at $r = 1.5r_g$. Contrary to the case of a black hole, even if a photon crosses the unstable circular orbit, $r = 1.5r_g$, it eventually scattered away from it.

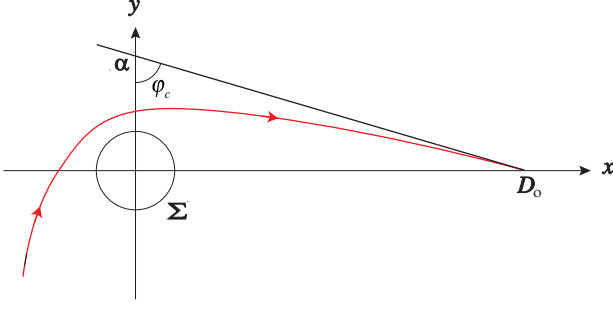


FIG. 5: The $z = 0$ plane in the 3-space $(x, y, z) = (r \cos \varphi \sin \theta, r \sin \varphi \sin \theta, r \cos \theta)$. The center of the gravastar is located at the origin and the observer at $(D_o, 0, 0)$. The intersection of the y -axis with the tangent to the ray at the observer is denoted by $(0, \alpha, 0)$. The integral constant φ_c corresponds to the angle indicated by this figure: $\tan \varphi_c = D_o/\alpha$.

IV. IMAGES OF OPTICAL SOURCES BEHIND A GRAVASTAR

A. Basic features of null geodesics coming to observer

In order to describe light trajectories, we define the rectangular coordinates $(x, y, z) = (r \cos \varphi \sin \theta, r \sin \varphi \sin \theta, r \cos \theta)$. We suppose that the center of the gravastar is located at the origin and the observer at $(D_o, 0, 0)$ ($\varphi = 0$). Figure 5 shows the $z = 0$ ($\theta = \pi/2$) plane. If we make a coordinate rotation appropriately, any trajectory can be put on this plane. On this plane, we denote the intersection of the y -axis with the tangent to the ray at the observer by $y = \alpha$. In this rectangular coordinate system the asymptotic solution (3.10) is rewritten as

$$x \cos \varphi_c + y \sin \varphi_c = \frac{L}{E}, \quad (4.1)$$

where the x -intercept and the y -intercept are given by

$$D_o = \frac{L}{E} \sec \varphi_c, \quad \alpha = \frac{L}{E} \operatorname{cosec} \varphi_c, \quad (4.2)$$

respectively. Recall that φ_c is an integral constant defined by (3.10). Because (4.2) indicates

$$\tan \varphi_c = \frac{D_o}{\alpha}, \quad (4.3)$$

we find that the integral constant φ_c corresponds to the angle indicated by Fig. 5.

Furthermore, taking the limit of $D_o \rightarrow \infty$, we obtain

$$\varphi_c \rightarrow \frac{\pi}{2}, \quad \alpha \rightarrow \frac{L}{E}. \quad (4.4)$$

Therefore, if D_o is large enough, we can regard L/E as the apparent length from the center as well as the impact parameter.

In our numerical analysis below, we put an observer at $D_o = 1000r_g$. Figure 6 shows several trajectories of

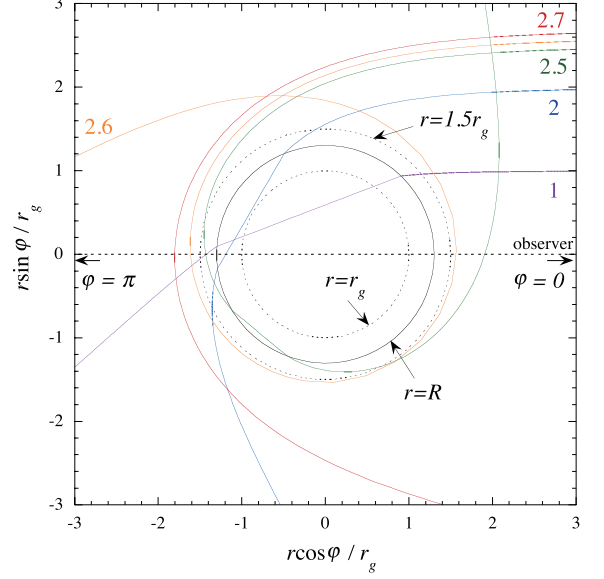


FIG. 6: Trajectories of photons which reach the observer for the model with $h = 0.4$ ($\tilde{R} = 1.303$). The observer is located at $r = 1000r_g$, $\varphi = 0$, the right side of the figure. We denote the positions of $r = r_g$ and $r = 1.5r_g$ by dotted lines for reference. We show five trajectories with $L/Er_g = 1, 2, 2.5, 2.6$ and 2.7 .

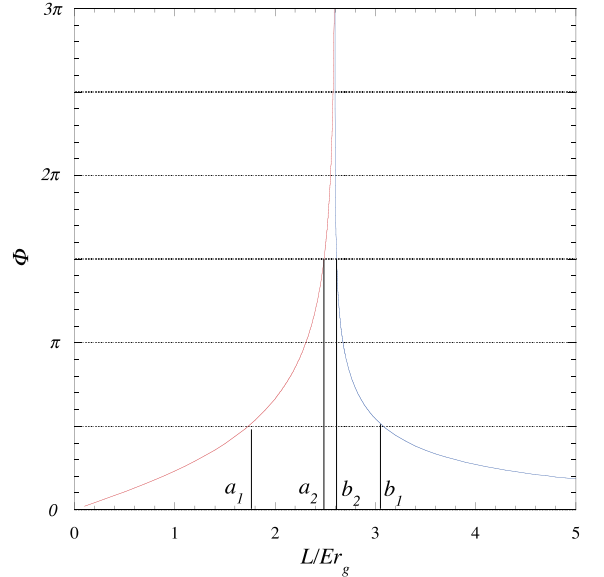


FIG. 7: Relation between the impact parameter L/E and the deflection angle Φ , which is defined by (4.5), for the model with $h = 0.4$ ($\tilde{R} = 1.303$). The observer is located at $\varphi = 0$, $r = 1000r_g$. The peak corresponds to the geodesics which wind infinite times on the unstable circular orbit $r = 1.5r_g$, and diverges at $L/Er_g = 1.5\sqrt{3} \approx 2.5981$. While the photons with $L/Er_g > 1.5\sqrt{3}$ (blue line) travel only in Schwarzschild background, the photons with $L/Er_g < 1.5\sqrt{3}$ (red line) pass through the gravastar interior. We denote the values of L/Er_g which satisfy $\Phi = \pi(n - 1/2)$ by a_n, b_n ($a_n < b_n$).

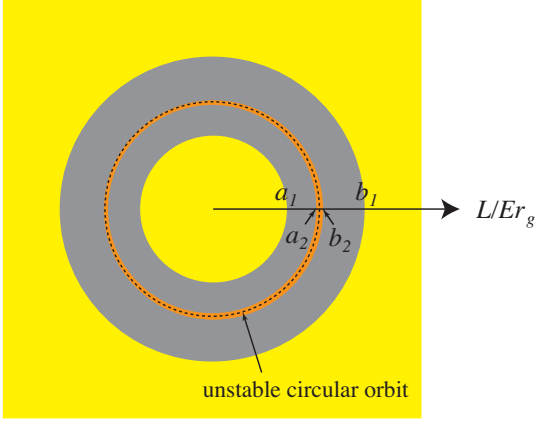


FIG. 8: Shadow cast by an infinite optical plane behind the gravastar with $h = 0.4$ ($\tilde{R} = 1.303$). This figure is depicted based on the numerical results in Fig. 7. In the yellow domains the photons emitted by the infinite plane come to the observer. We do not take account of light-dark contrast, which is generated by gravitational redshift of the photons. In the dark domains $[a_1, a_2]$ and $[b_1, b_2]$, no photon comes to the observer from the optical infinite plane. In the orange domain $[a_2, b_2]$ there are infinite numbers of bright and dark rings. The dotted circle corresponds to the unstable circular orbit in Schwarzschild background.

photons which reach the observer for the gravastar with $h = 0.4$.

To understand more clearly how trajectories depend on the impact parameter L/E , we define the deflection angle Φ by

$$\Phi \equiv \varphi(r_g = 1000r_g) - \pi, \quad (4.5)$$

which denotes the deflection measured from the opposite direction to x -axis. This Φ is convenient for the next subsection. Figure 7 shows the relation between Φ and L/E . The peak corresponds to the geodesics which wind infinite times on the unstable circular orbit $r = 1.5r_g$, and diverges at $L/Er_g = 1.5\sqrt{3} \approx 2.5981$. While the photons with $L/Er_g > 1.5\sqrt{3}$ (blue line) travel only in Schwarzschild background, the photons with $L/Er_g < 1.5\sqrt{3}$ (red line) pass through the gravastar interior. In pure Schwarzschild spacetime only geodesics with $L/Er_g > 1.5\sqrt{3}$ (blue line) exist. We also denote the values of L/Er_g which satisfy

$$\Phi = \pi \left(n - \frac{1}{2} \right), \quad (n = 1, 2, \dots). \quad (4.6)$$

by a_n, b_n ($a_n < b_n$). For convenience we also define a_0 as $a_0 = 0$.

In the following we consider two types of optical sources behind the gravastar: an infinite optical plane and a companion.

B. Image of an infinite optical plane behind a gravastar

An infinite plane is a simplified model of an extended gas behind the gravastar. Because the deflection angle

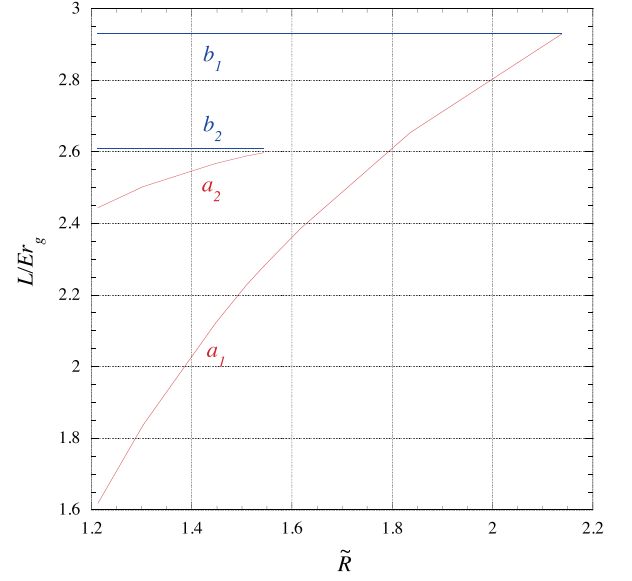


FIG. 9: Ring sizes of shadows cast by backlight for several models. b_1 and b_2 are independent of or \tilde{R} as long as they exist, because they are determined by Schwarzschild geometry. a_1 and a_2 are increasing functions of \tilde{R} , and they have upper limits, $a_2 < b_2 \approx 2.61$ and $a_1 < b_1 \approx 2.93$.

of photons which emit by the infinite plane and come to the observer should be in the range,

$$a_{2n} < \Phi < a_{2n+1} \quad (n = 0, 1, 2, \dots), \quad (4.7)$$

Figure 7 enables us to depict the shadow of the gravastar with $h = 0.4$, as shown in Fig. 8.

The main feature is that a bright disk in $L/Er_g < a_1$ is surrounded by a dark domain $a_1 < L/Er_g < a_2$. In the dark domains $[a_1, a_2]$ and $[b_1, b_2]$, no photon comes to the observer from the optical infinite plane. In the orange domain $[a_2, b_2]$ there are infinite numbers of bright and dark rings. While the image outside the dotted circle is common to pure Schwarzschild spacetime, the image inside it is unique to the gravastar. Here we do not take account of light-dark contrast, which is generated by gravitational redshift of the photons.

Because a_1 corresponds to the geodesics whose deflection angle is $\pi/2$, the whole landscape behind the gravastar is reduced in the central yellow disk. Hence, we can interpret the gravastar as a concave lens with much reduction rate.

Next, we discuss how the ring sizes depend on the model parameters. Among the three parameters h , s and \tilde{R} , only one is independent, as shown in Fig. 2. Therefore we show the ring sizes a_1 , a_2 , b_2 and b_1 as a function of \tilde{R} in Fig. 9. Here we extend our analysis to the case where there is no unstable circular orbit of photons, i.e., $\tilde{R} > 1.5$. b_1 and b_2 are independent of h or \tilde{R} as long as they exist, because they are determined by Schwarzschild geometry. a_1 and a_2 are increasing functions of \tilde{R} , and they have upper limits, $a_2 < b_2 \approx 2.61$ and $a_1 < b_1 \approx 2.93$.

There are merging points of a_i and b_i , which we denote $\tilde{R} = \tilde{R}_i$. We numerically find that $\tilde{R}_2 \approx 1.58$ and

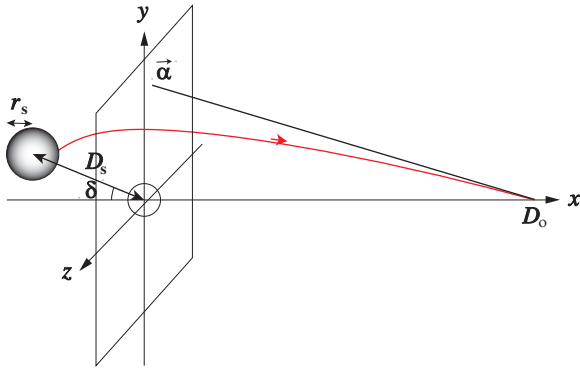


FIG. 10: Setting of our analysis of gravitational lens effects. We suppose a companion behind a gravastar. We put the gravastar's center and the companion's center at the origin and on the $z = 0$ -plane, respectively. We denote the distance between the companion's center and the gravastar's center by D_s and the radius of the companion by r_s . The angle δ is defined as the angle between the direction of the companion's center and the opposite direction to x -axis. The image $\vec{\alpha} = (\alpha_y, \alpha_z)$ is defined as the intersection of the $x = 0$ plane with the tangent to the ray at the observer.

$\tilde{R}_1 \approx 2.14$. The orange domain $[a_2, b_2]$ in Fig. 8 disappears when $\tilde{R} > \tilde{R}_2$ and the dark domain $[a_1, b_1]$ disappears when $\tilde{R} > \tilde{R}_1$. The merging points are determined by the Schwarzschild geometry as follows. For the photon trajectory of b_i , there is the closest point to the gravastar's center, whose position we denote by $r_+ = \min[r_+(b_i)]$. The trajectory of b_i cannot exist if the gravastar's radius is larger than $\min[r_+(b_i)]$. We thus obtain the relation,

$$\tilde{R}_i = \min \left[\frac{r_+(b_i)}{r_g} \right]. \quad (4.8)$$

C. Image by a companion star behind a gravastar

Next, supposing that a companion star rotates around a gravastar, we investigate its image caused by gravitational lens effects. Figure 10 shows the setting of our numerical analysis. We suppose the companion is located behind the gravastar. We put the gravastar's center and the companion's center at the origin and on the $z = 0$ -plane, respectively. We denote the distance between the companion's center and the gravastar's center by D_s and the radius of the companion by r_s . The angle δ is defined as the angle between the direction of the companion's center and the opposite direction to x -axis. The image $\vec{\alpha} = (\alpha_y, \alpha_z)$ is defined as the intersection of the $x = 0$ plane with the tangent to the ray at the observer.

Figure 11 shows an example of the images of the companion projected onto the $x = 0$ plane. The center of the gravastar is fixed at the origin. We choose $D_s = 10r_g$ and $r_s = 2r_g$. We show four snapshots when $\delta = 30^\circ, 20^\circ, 12^\circ$ and 10° . The red images correspond to geodesics which pass through the gravastar, while the blue ones to those which pass only through Schwarzschild

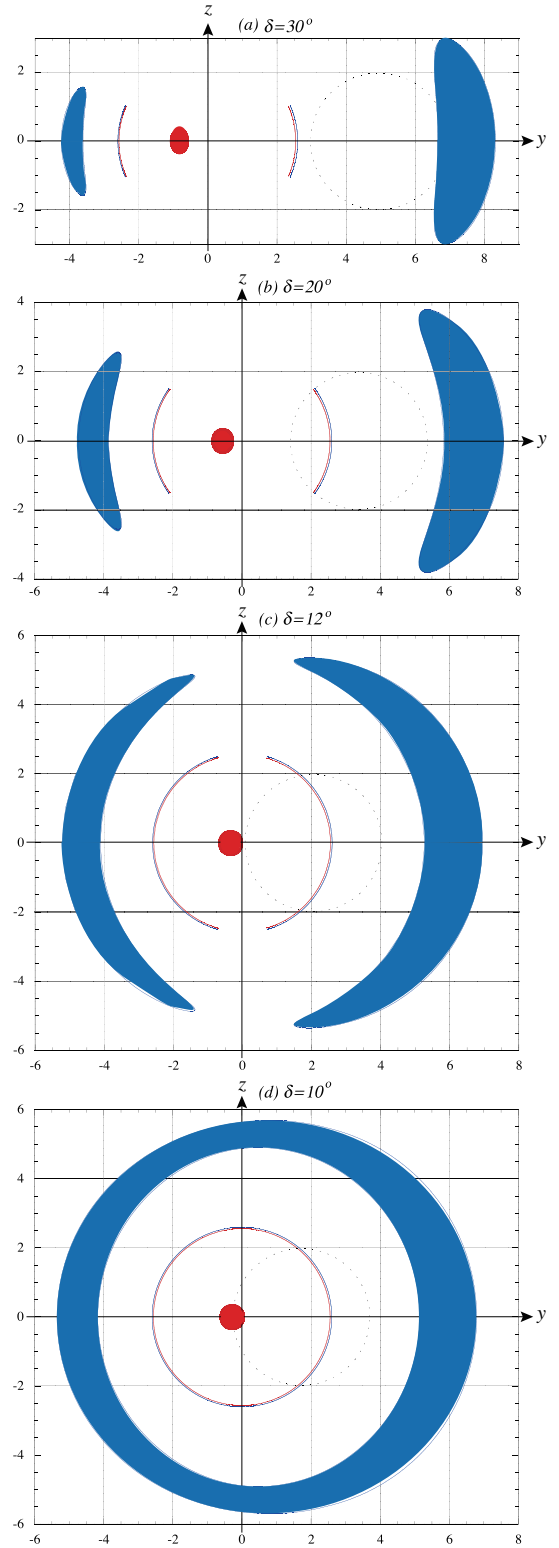


FIG. 11: Example of the gravitational lens images of the companion projected onto the $x = 0$ plane. We put the gravastar with $h = 0.4$ ($\tilde{R} = 1.303$) at the origin. We choose $D_s = 10r_g$ and $r_s = 2r_g$. We show four snapshots when $\delta = 30^\circ, 20^\circ, 12^\circ$ and 10° . The blue images correspond to geodesics which pass only through Schwarzschild background, while the red ones to those which pass through the gravastar. The dotted lines indicate the image in the absence of the gravastar. We do not take account of light-dark contrast, which is generated by gravitational redshift of the photons.

background. The dotted circles indicate the image in the absence of the gravastar. Here we do not take account of light-dark contrast, which is generated by gravitational redshift of the photons. The characteristics of the gravastar are the red images: a disk in the center and arcs in the sides. Actually, there are infinite numbers of arcs between the red arc and the blue arc. As the companion moves, the central disk moves in the opposite direction. As the companion approaches the center (the x -axis), the arcs in both sides become longer, and finally they are combined into one image, like the blue images in the Schwarzschild spacetime.

It is instructive to compare the image of the companion in Fig. 11 with that of the infinite plane in Fig. 8. We can interpret that the red circle and the thin arcs in Fig. 11 are in the yellow disk and in the orange domain in Fig. 8, respectively. Because the orange domain disappears when $\tilde{R} > \tilde{R}_2 \approx 1.58$, the blue and red thin arcs also disappear accordingly.

These lensing phenomena are interesting and give definite observational predictions. We are afraid, however, that there may be little chance of observing images like the red ones for the following reason. In Fig. 11 the red disk may be observable but are much smaller than the “original image” represented by the dotted line. This reduction takes place because the gravastar acts as a concave lens with much reduction rate, as discussed in Sec. IV.B.

V. CONCLUDING REMARKS

Direct observation of black holes usually means observation of geometry in the vicinity of unstable circular orbits of photons. Therefore, if there are super-compact objects which possess the unstable circular orbits, it may be difficult to distinguish them from black holes by observing photons. As a model of super-compact objects, we have considered a model of gravastars. We have discussed whether we can distinguish gravastars from black holes by electromagnetic observations. This work is a kind of extension of Chirenti and Rezzolla, who discussed how to tell a gravastar from a black hole by gravitational wave observations.

For definiteness, we have adopted a spherical thin-shell model of a gravastar developed by Visser and Wiltshire, which connects interior de-Sitter geometry and exterior Schwarzschild geometry. We have found that unstable circular orbits of photons can appear around the gravastar.

Next, we have investigated the optical images of the

gravastar possessing unstable circular orbits, with assuming the optically transparent surface of it and two types of optical sources behind the gravastar: (i) an infinite optical plane and (ii) a companion star. The main feature of the image of (i) is that a bright disk and a dark thick ring surrounding the disk appear in the center of the region which would be completely dark if the compact object was not the gravastar but Schwarzschild black hole. Also in the case (ii), a small disk and arcs around the disk appear in the region which would be completely dark for Schwarzschild black hole.

Because characteristic images appear inside the gravastar in both cases, we could tell the difference between a black hole and a gravastar with high-resolution VLBI observations near future. It is also important to study the possibility of other quasi-black-hole objects and their observational consequences not only to discover those exotic objects but to identify black holes observationally.

Our original interest is in a gravastar which possesses unstable circular orbits of photons ($R < 1.5r_g$) because the shadow of a gravastar with $R > 1.5r_g$ is different from that of a black hole even if the surface is black and does not emit electromagnetic waves. (Photons passing through the region $1.5r_g < r < R$ make a difference in shadow between a gravastar and a black hole.) Aside from our original interest, we have extended our analysis to the case of $R > 1.5r_g$ and find that a gravastar with $1.5r_g < R < 2.14r_g$ shares the above main feature: a bright disk and a dark thick ring surrounding the disk appear in the image (i).

Finally, we make a brief comment on the “reflection” effect of a gravastar. As shown in Figs. 6 and 7, there are geodesics which start at an observer, make a π rotation about the gravastar, and then end up at the observer. That is, the observer on the Earth could detect photons which leave the Sun and travel around the gravastar. These photons exist both in the dark domains $[a_1, a_2]$ and $[b_1, b_2]$ in Fig. 8. In the dark domains photons which reach the observer come from the front side; therefore, the dark domains may be called “mirrors” rather than “shadows”. Such reflection phenomena have been discussed for black holes and called retro-MACHO [8]. What we find here is reflection phenomena also happen to photons which penetrate gravastars.

Acknowledgments

H.S. was supported by Japan Society for the Promotion of Science (JSPS), Grant-in-Aid for Scientific Research (KAKENHI, Exploratory Research, 26610050).

[1] M. Miyoshi, J.K. Ishitsuka, S. Kamenno, Z. Shen and S. Horiuchi, Prog. Theor. Phys. Suppl. **155**, 186 (2004); H. Hirabayashi et al., arXiv:astro-ph/0501020; S. Doeleman et al., Nature **455**, 78 (2008); M. Miyoshi et al., Publication of National Astronomical Observatory Japan **10**, 15 (2007); M. Miyoshi et al., Astronomical Society of the

Pacific, p.279 (2011).
[2] P.O. Mazur and E. Mottola, arXiv:gr-qc/0109035; Proc. Nat. Acad. Sci. **101**, 9545 (2004).
[3] C.B.M.H. Chirenti and L. Rezzolla, Class. Quant. Grav. **24**, 4191 (2007).
[4] A.E. Broderick and R. Narayan, Class. Quant. Grav. **24**,

- 659 (2007).
- [5] M. Visser and D.L. Wiltshire, *Class. Quantum Grav.* **21**, 1135 (2004).
- [6] W. Israel, *Nuovo Cimento* **44B**, 1 (1966).
- [7] S. K. Blau, E. I. Guendelman, and A. H. Guth, *Phys. Rev. D* **35**, 1747 (1987).
- [8] D.E. Holz and J.A. Wheeler, *Astrophys. J.* **578**, 330 (2002); F. DePaolis, A. Geralico, G. Ingrosso and A.A. Nucita, *Astron. Astrophys.* **409**, 809 (2003). F. DePaolis, A. Geralico, G. Ingrosso, A.A. Nucita and A. Qadir, *Astron. Astrophys.* **15**, 1 (2004).